Colloids and Surfaces A 524 (2017) 66–70

Contents lists available at ScienceDirect

Colloids and Surfaces A

journal homepage: www.elsevier.com/locate/colsurfa

Mesoporous metal-oxide-semiconductor capacitors detect intra-porous fluid changes

Rocío Gimenez[a], Diana C. Delgado[a], Félix Palumbo[a,b,*], Claudio L.A. Berli[c,*], Martín G. Bellino[a,*]

[a] Comisión Nacional de Energía Atómica, CONICET, Av. Gral. Paz 1499, San Martín, Buenos Aires, Argentina
[b] Departamento de Ingeniería Electrónica, Universidad Tecnológica Nacional (UTN), Medrano 951, Buenos Aires, Argentina
[c] INTEC (Universidad Nacional del Litoral-CONICET) Predio CCT CONICET Santa Fe, RN 168, 3000, Santa Fe, Argentina

ARTICLE INFO

Keywords:
Mesoporous films
Nano-fluidics
MOS-capacitors
Evaporation

ABSTRACT

Real-time measurements of fluidic phenomena inside nano/mesoporous films offer an alternative way to study fundamental processes, as well as to explore novel applications. Most current techniques use optical measurement methods or microgravimetric approaches. Here it is shown that a metal-oxide-semiconductor (MOS) capacitor can be used to detect fluidic transport inside mesoporous networks. The MOS stack, which consists of two contacts (Cu and silicon) separated by a supramolecularly templated mesoporous oxide film to form a MOS capacitor, detects fluid changes that can be quantified from an effective permittivity model of mesoporous structures interacting with a fluid. The device was used to monitor liquids infiltration and subsequent evaporation in both titania and silica mesoporous films. It was observed how the evaporation dynamics significantly depends on film characteristics and fluid properties.

1. Introduction

Scientific interest in the intersection of micro- and nanotechnologies with fluidic behavior has been focused on providing new tools to study fluidic transport in nano-systems [1,2]. Fabrication based on these techniques offers the potential to develop integrated devices and allows for new opportunities for the nanoscale analysis of flow behavior. Progress in designing optimized nanostructures/devices needs a clear understanding of fluid dynamics behavior [3,4]. Mesoporous thin films-based devices are used in the production and purification of drugs [5], the sensing of diverse molecules [6], biofuel cell developments [7], photovoltaic devices [8], and other catalytic applications [9,10]. In all such applications, the assessment of fluid dynamics in the porous networks is required. Existing few techniques for the direct measurement of fluids in mesoporous films include ellipsometric methods that induce change in the polarization state of a linearly polarized collimated light beam after being reflected by the film [11], or methods that detect variations in the specular reflectance [12]. In contrast, the surface Plasmon resonance technique allows for an indirect measurement of solvent evaporation by inserting metallic nanoparticles into mesoporous films [13]. Also, through changes in the vibrational frequency of a quartz crystal slide onto which a film was deposited, fluid imbibition analysis was achieved [14]. The development of new experimental tools to describe and predict fluid dynamics in mesoporous films is eagerly awaited.

A simple capacitor can be made of a metal electrode, an oxide film and a semiconductor substrate (MOS) [15]. The MOS system has been studied extensively during the last decades because it is directly related to most planar devices and integrated circuits. Devices including MOS systems have applications in tasks as diverse as signal processing, electronic switch and sensing [16,17]. The integration of such nano-fluidic devices in the mature MOS technology increases significantly its technological applications. Such a structure, in which a porous oxide slab would be sandwiched between the semiconductor and metal contact, should present a sharp and intense response to pore filling and emptying, taking into account the relatively large permittivity of liquids, mainly water. Here, we have fabricated a fluidic-dynamics interrogation method based on capacitance measurements than enables a MOS stack to detect changes in fluids within mesoporous films.

2. Experimental section

2.1. Fabrication of mesoporous MOS stacks

Crack-free mesoporous titania (TF) and silica (SF) thin films were prepared by the evaporation induced self-assembly (EISA) strategy using an inorganic precursor and a surfactant template in ethanol solution [7,18–20]. The detail techniques for the preparation of the

* Corresponding authors.
E-mail addresses: felix.palumbo@conicet.gov.ar (F. Palumbo), cberli@santafe-conicet.gov.ar (C.L.A. Berli), mbellino@cnea.gov.ar (M.G. Bellino).

http://dx.doi.org/10.1016/j.colsurfa.2017.04.035
Received 25 January 2017; Received in revised form 17 April 2017; Accepted 18 April 2017
Available online 20 April 2017

films have been reported elsewhere [18–20]. $TiCl_4$ and $Si(OEt)_4$ (TEOS) were used as inorganic precursors for titania and silica films respectively, and Pluronics F127 was selected as the surfactant template. The titania precursor solution was composed of $TiCl_4$:EtOH:H_2O:F127 with a molar ratio of 1:40:5:0.0075 while the silica precursor solution was composed of TEOS:EtOH:H_2O:F127 with a ratio of 1:40:5:0.0075. Mesoporous titania films were deposited by dip-coating at 1.5 mm/s on a p-type silicon substrate at RH of 30%, and silica films were spin-coated at 3000 rpm also on p-type silicon substrates at relative humidity (RH) of 30%. After deposition, the films were placed in 50% RH chamber overnight, then they were subjected to a consolidation thermal treatment, which consisted of 24 h at 60 °C, 24 h at 130 °C, and finally calcined at 350 °C for 2 h (temperature ramp of 1 °C/min) in order to remove the templating agent. The Cu gate electrodes (200 nm thick and 1 mm in diameter) were deposited by sputtering and patterned using a physical mask. Cu was selected as the contact material because of its high electrical conductivity, reducing the resistance of the experimental set-up.

2.2. MOS stacks characterization

For the mesoporous film characterization, pore size distributions were measured by Environmental Ellipsometric Porosimetry (EEP) [11]. Film thickness and reflective index values were obtained from the ellipsometric parameters ψ and Δ at each P/P_0 (P_0 being the saturation water pressure), which was varied from 0 to 1 using a SOPRA GES5A ellipsometer. Film porosity φ was evaluated by the WinElli 2 software (SopraInc), which transforms the variation of the refraction index with P/P_0 into filled pore volume by using a three constituent Bruggeman Effective Medium Approximation (BEMA) treatment. Pore and neck size distributions are derived according to a Kelvin model. Micrographs were obtained using a ZEISS LEO 982 GEMINI field emission electron microscope in the secondary-electron mode, using an in-lens detector to improve resolution.

The water adsorption studies were based on the variations of the capacitance when MOS stacks were exposed to different vapor concentrations (20–45%) in a closed chamber. On the other hand, water imbibition-evaporation experiments were carried out by placing a drop of water (2 μl) on the mesoporous film, 300 μm apart from the electrode at 25 °C and 40–45% relative humidity. Capacitance–Voltage (C-V) measurements were recorded using an Agilent 4285A LCR meter.

3. Results and discussion

3.1. Structural and MOS-capacitor characterization

The design comprises a MOS defined by two contacts (silicon and Cu) separated by a supramolecularly template mesoporous oxide film. Fig. 1 shows typical SEM images and elipsoporosimetry-derived pore size distribution of F127-templated silica and titania films (labeled SF and TF respectively) where both the mesostructure and uniform pore size can be clearly observed. The textural characteristics of these films are summarized in Table 1.

The capacitance-voltage (CV) characteristics of both stack structures showed well resolved typical MOS capacitance behavior [15] (Fig. 2). When voltage is applied on the metal contact, the semiconductor minority carriers are modulated changing the density of the charge on the semiconductor surface next to the dielectric. Being the MOS capacitance defined as small-signal differential of charge with respect to voltage or potential, it is such charge modulation that affects the total capacitance of the MOS stack in the way observed in Fig. 2. In particular, when a negative voltage is applied to the gate of a p-type MOS capacitor, the metal Fermi level (i.e., electron energy) raises with respect to the silicon Fermi level and creates an electric field in the oxide that would accelerate a negative charge toward the silicon substrate. A field is also induced at the silicon surface in the same

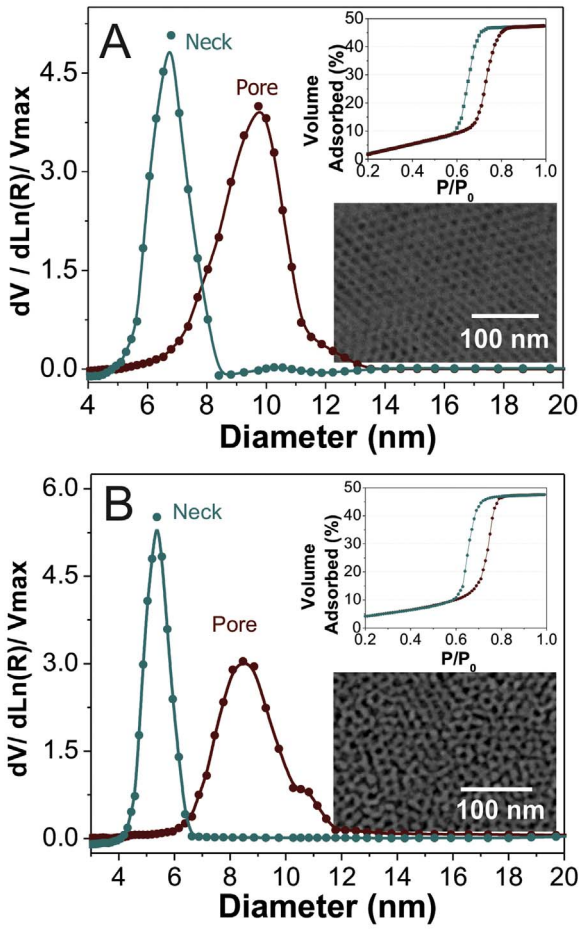

Fig. 1. Structural mesoporous film characterization of SF (a) and TF (b) samples tested in this study. Pore size distribution (red line) and neck size distribution (blue line) obtained by water adsorption–desorption isotherms at 298 K (see upper insets). SEM images of the mesoporous films tested in this study (see lower insets). (For interpretation of the references to colour in this figure legend, the reader is referred to the web version of this article.)

Table 1
Structural data of the mesoporous silica (SF) and titania (TF) thin films.

Sample	Thickness (nm)	Porosity (%)	Pore size (nm)	Neck size (nm)
SF	170	47	10	7
TF	105	48	9	6

direction as the oxide field. This results in a hole concentration much higher at the surface than the equilibrium hole concentration in the bulk [15]. One can think of the excess holes as being attracted toward the surface by the negative gate voltage. An equal amount of negative charge appears on the metal side of the MOS capacitor, as required for charge neutrality. Considering the differential of charge with respect to voltage in accumulation condition (where excess holes are accumulated at the surface; i.e. negative bias for p-type Si substrate), the MOS capacitance rapidly approaches C_m which is the mesoporous layer capacitance defined by $C_m = \varepsilon_m/t_m$; where ε_m is the layer permittivity, and t_m the thickness of the dielectric layer.

3.2. Fluid-detecting system

The mesoporous layer should act as a gate dielectric in the MOS stack which is ultra-sensitive to the transport of fluid through it due to variations in the dielectric constant. As water infiltration/condensation fills the pores or evaporation empties them, the effective dielectric

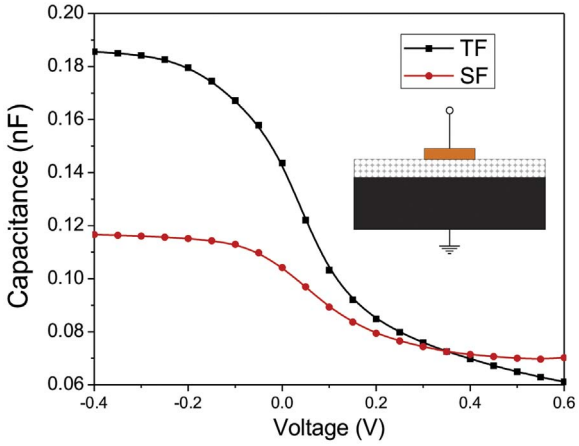

Fig. 2. Typical capacitance measurements as a function of applied voltage at 500 kHz and 45% RH for the mesoporous MOS stacks used in this work. Inset: A schematic of a MOS Capacitor consisting of a mesoporous oxide layer.

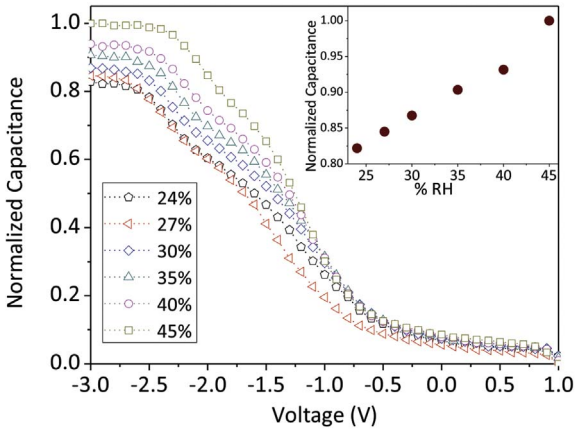

Fig. 3. C-V measurements of a mesoporous silica MOS stack exposed at different pressures of water vapor in the closed chamber.

constant of the mesoporous film changes since it is a composite material layer made by the macroscopic mixture of 3 homogeneous components (air, liquid and oxide) [21]. Accordingly, the achieved effective dielectric constant is modulated by the fraction of filled pores. Briefly, the sensing principle is based on the acquisition of capacitance in accumulation condition for a given time and the modeled quantification of the amount of liquid inside the pores. The fabricated devices were then validated using different water vapor concentrations in a closed chamber (See Fig. 3). In accumulation condition, capacitance increased following a linear dependence with relative humidity (RH) up to 50%. We also observed that this process is reversible, demonstrating that the water vapor presence inside the mesoporous network follows external pressure changes. Control experiments were carried out for the non-template layer where no capacitance responses to environmental changes were observed. These results show the capability of detecting water pressure fluctuations inside mesoporous films.

We then explored the phenomena that takes place when a sessile drop of liquid (2 µl) is deposit onto a mesoporous film. Placing a drop 300 µm beside the metal contact leads to a large increase in capacitance for both absolute ethanol and Milli-Q water (See Fig. 4). We attribute this observation to spontaneous wetting of the mesoporous matrix under the electrode area [22,23]. It is worth mentioning that the saturation level is different for each fluid, since water and ethanol hold different permittivity resulting in different C_m at the same volume fractions of the pure phases. Then, there is a second, slower phase in which the capacitance in accumulation decreases towards the initial magnitude. We associate this stage with the evaporation of the liquid.

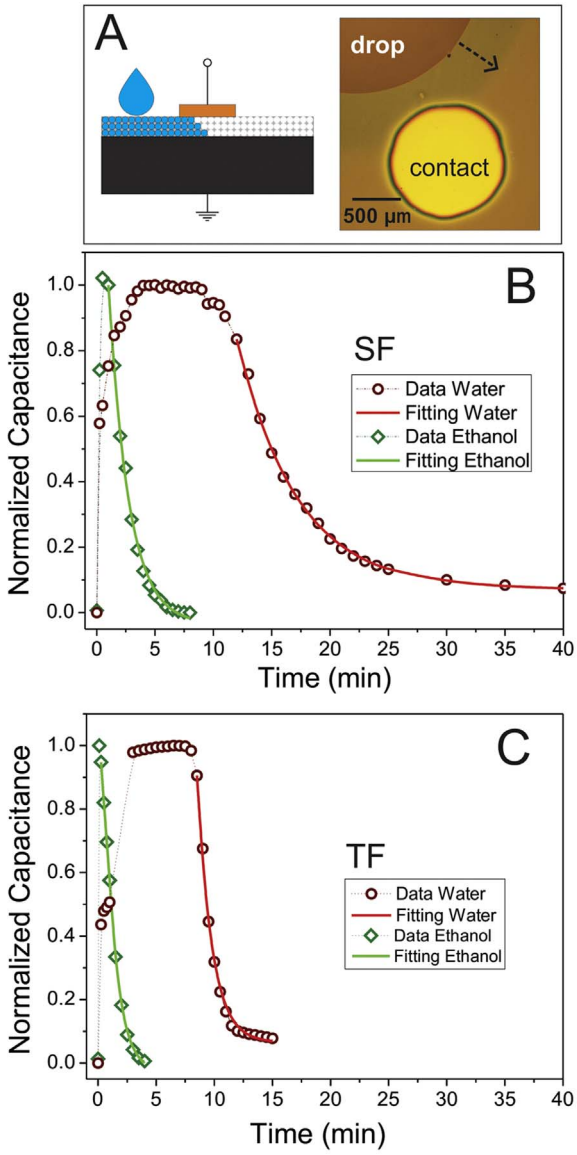

Fig. 4. Upper Frame: Schematics of the experimental setup for imbibition of water into mesoporous MOS stacks and illustrative optical image of the contact and water drop (a). The arrow indicates the water imbibition front. Lower Frame: Capacitance in accumulation condition versus time after sessile drops of water (red) and ethanol (green) were deposited onto SF (b) and TF (c) surfaces. For a better comparison both curves are normalized. Symbols represent experimental data and solid lines are the prediction of Eq. (4) for the evaporation stage. Dotted lines are guides for the eye during the imbibition step. (For interpretation of the references to colour in this figure legend, the reader is referred to the web version of this article.)

Although changes are abrupt, we consistently find that capacitance increases during imbibition, and decreases in the evaporation stage. When different solvents are compared, all the curves present similar shape but with noticeable differences regarding the duration ofeach-stage. These differences arise because each liquid present different properties, such as viscosity and vapor pressure. The results in Fig. 4 demonstrate the ability of detecting the imbibition and evaporation behavior of the fluid inside the mesoporous network.

3.3. Evaporation process model

In order to analyze the evaporating process, we have developed a simple model for the time-dependent effective permittivity of mesoporous structures. The microscopic geometry of the ultra-thin mesoporous layer in the MOS stacks was represented as plane parallel layer

perpendicular to the Si substrate. The model adopted consists of 3 capacitors connected in parallel corresponding to the 3 pure phases of the stack. It is worth mentioning that the contribution of each capacitor will depend on the volume fraction of the pure phases: f_l, f_a, and f_s, where sub-indexes l, a, and s stand for liquid, air, and solid, respectively. The experimental capacitance vs. time plot allows us to calculate the variation of the effective relative permittivity as the evolution of the filled pore fraction, as explained in what follows. Thus, the effective permittivity of an inhomogeneous medium can be determined given the properties of its constituents under certain assumptions. In our case, we apply an equation for a weighted three-component dielectric medium, based on an effective medium theory [21], that is $\varepsilon_{\text{eff}} = f_s\varepsilon_s + f_l\varepsilon_l + f_a\varepsilon_a$. We consider our inhomogeneous medium to be composed of three different constituents, namely, the material of which the pore walls are made of, the adsorbed solvent present in the pores, and air. Both f_l and f_a vary in time during condensation-infiltration-evaporation processes, while the relation $f_l(t) + f_a(t) = \phi$ holds, being $\phi$the porosity of the medium. Here it is useful to introduce the saturation S, which is equal to the fraction of the pore space occupied by the test liquid. Thus, the liquid volume fraction is $\phi\, S(t)$, and the time-dependent effective electrical permittivity can be written,

$$\varepsilon_{\text{eff}}(t) = (1-\phi)\varepsilon_s + \phi S(t)\varepsilon_l + \phi[1 - S(t)]\varepsilon_a \quad (1)$$

This equation reduces to two terms in the limits of either fully embedded ($S = 1$), or fully empty pores ($S = 0$); the last situation corresponds to an oven-dried film, since in standard conditions the mesoporous material has an S level in equilibrium with ambient RH. Because of the large difference between the dielectric constant of the liquids and the air (80 vs. 1 for water) [24] an improved sensibility can be expected in relation to optical/other methods.

Next step consists in modeling the capacitance variations during the evaporation of the test liquid. For this purpose, one may assume that the evaporation rate per unit area of the wetted surface, $\dot{m}_{\text{ev}} = |dm/dt|/A$ is constant for a given liquid, room temperature, and RH. This macroscopic approach has been employed to describe evaporation in porous media with different microstructure length scales: walls [25], metallic weaves [26], and nanowire networks [27]. If one further assumes that evaporation predominantly takes place in the upper film surface (taking into account that the film thickness h is negligibly small and that the bottom side of the film is isolated), the diminution rate of the wetted area A_w can be written as $\rho\phi h dA_w/dt = -\dot{m}_{\text{ev}}A_w$, where ρ is the fluid density. Dividing both sides of this equation by the control area of the system leads to following expression for the diminution rate of S due to evaporation,

$$\frac{dS}{dt} = -\frac{\dot{m}_{\text{ev}}}{\rho\phi h}S \quad (2)$$

During the time interval where evaporation is the only relevant process, the time-dependent saturation comes from the straightforward integration of Eq. (2),

$$S(t) = S_0\exp(-t/\tau) \quad (3)$$

where $S_0 = S(t = 0)$ is the initial saturation value, and $\tau = h\rho\phi/\dot{m}_{\text{ev}}$ is defined as a characteristic evaporation time. It is worth noting that, although evaporation produces heat exchange, which is particularly effective in thin films, here the system is considered to be isothermal, as a first approximation. Under these conditions, introducing Eq. (3) into Eq. (1) yields the effective dielectric constant of the composite material, as a function of time, during liquid evaporation:

$$\varepsilon_{\text{eff}}(t)/\varepsilon_0 = (1-\phi)\varepsilon_s + \phi S_0\exp(-t/\tau)\varepsilon_l + \phi[1 - S_0\exp(-t/\tau)]\varepsilon_a \quad (4)$$

Therefore, knowing the vacuum permittivity ε_0, the dielectric constant of the mesoporous material ($k_w = 3.9$ for silica and $k_w = 33$ for titania) [28], the test liquid (k_s, taken as 80 and 25 for water and ethanol respectively), [22] and the air ($k_a = 1$), Eq. (4) allows one to estimate τ and S_0 by fitting experimental curves of capacitance vs. time during the evaporation stage. Results are shown in Table 2. Also in this table, the evaporation rate ($\dot{m}_{ev} = h\rho\phi/\tau$) was calculated from τ and the respective system parameters reported in Table 1. In addition, $\rho = 1000\ \text{kg/m}^3$ and $\rho = 789\ \text{kg/m}^3$ were used for water and ethanol, respectively. The evaporation rates obtained for both solvents are lower than the result achieved with the bulk evaporation (around 10^{-4}–$10^{-5}\ \text{kg/m}^2\,\text{s}$, depending on experimental conditions; see for example ref. [29]). These resulting lower evaporation rates are expected as suggested in literature [30], taking into account the confinement effects into the nanoporous matrix, and mainly the presence of the electrode, which avoids the wetted film exposition to the open air. From these experiments, it can be also observed that the evaporation clearly depends on the nature of the specific interactions between the oxide as well as the solvent and film morphology [30]. These results show that with this approach, it is possible to estimate the evaporation rate of different solvents from mesoporous oxide thin films and to differentiate between solvents. Table 2 also shows the mesopore filling fraction (MFF) calculated for the systems described above. It can be observed that mesoporous films show average filling fractions below 30%. It is important to note that the model assumes that this percentage is equal throughout the contact area, but certainly there is an imbibition front [22,23], so there is a small zone were most pores are filled, while in the rest of the area many, if not all, pores remain principally empty (See Fig. 4a). Together these results demonstrate that a MOS platform with mesoporous architecture is able to detect fluid transport into the mesopores, even if the procedure has not been yet fully optimized.

Table 2
Parameters of Eq. (4) for the curves plotted in Fig. 4, and derived values of evaporation rate and mesopore filling fraction.

Sample	Liquid	τ (s)	$\dot{m}_{\text{ev}}(\text{kg/sm}^2) \times 10^{-7}$	S_0	MFF (%)
SF	Water	308	2.5	0.02	4
SF	Ethanol	103	5.9	0.06	13
TF	Water	75	6.7	0.09	18
TF	Ethanol	56	7.1	0.12	25

4. Conclusions

In summary, we introduced MOS capacitors as a robust yet versatile scaffold to study fluid behavior within mesoporous films. Additionally, the evaporation of the adsorbed solvent can be monitored and analyzed by a simply model of the MOS capacitance as a function of time. We believe that this is a first step towards a wide-ranging field of MOS mesochips that will offer a different perspective on fundamental problems in nanofluidics as well as novel sensor devices.

Acknowledgments

RG and DCD acknowledge their doctoral fellowships from CONICET, Argentina. This work was supported by CONICET (PIP-0363) and ANPCyT (PICT-2015-1051 and PICT-2012-2969), Argentina. The capacitance measurements were performed in the Lab. de Mediciones Eléctricas − Depto. de Energía Solar − CNEA.

References

[1] R.B. Schoch, J. Han, P. Renaud, Transport phenomena in nanofluidics, Rev. Mod. Phys. 80 (2008) 839–883.
[2] W. Sparreboom, A. Van Den Berg, J. Eijkel, Principles and applications of nanofluidic transport, Nat. Nanotechnol. 4 (2009) 713–720.
[3] T.M. Squires, S.R. Quake, Microfluidics Fluid physics at the nanoliter scale, Rev. Mod. Phys. 77 (2005) 977–1026.
[4] C.L.A. Berli, M. Mercuri, M.G. Bellino, Modeling the abnormally slow infiltration rate in mesoporous films, Phys. Chem. Chem. Phys. 19 (2017) 1731–1734.
[5] M. Suh, J.H. Lee, J.Y. Park, U. Lee, Y.U. Kwon, D.J. Kim, A mesoporous silica thin

film as uptake host for guest molecules with retarded release kinetics, ChemPhysChem 9 (2008) 1402–1408.
[6] W. Yantasee, Y. Lin, X. Li, G.E. Fryxell, T.S. Zemanian, V.V. Viswanathan, Nanoengineered electrochemical sensor based on mesoporous silica thin-film functionalized with thiol-terminated monolayer, Analyst 128 (2003) 899–904.
[7] M.G. Bellino, G.J.A.A. Soler-Illia, Nano-designed enzyme-functionalized hierarchical metal-oxide mesoporous thin films: en route to versatile biofuel cells, Small 10 (2014) 2834–2839.
[8] S.S. Soni, M.J. Henderson, J.F. Bardeau, Gibaud, Visible-light photocatalysis in titania-based mesoporous thin films, Adv. Mater. 20 (2008) 1493–1498.
[9] P. Innocenzi, L. Malfatti, Mesoporous thin films: properties and applications, Chem. Soc. Rev. 42 (2013) 4198–4216.
[10] C. Sanchez, C. Boissiere, D. Grosso, C. Laberty, L. Nicole, Design synthesis, and properties of inorganic and hybrid thin films having periodically organized nanoporosity, Chem. Mater. 20 (2008) 682–737.
[11] C. Boissiere, D. Grosso, S. Lepoutre, L. Nicole, A.B. Bruneau, C. Sanchez, Porosity and mechanical properties of mesoporous thin films assessed by environmental Ellipsometric porosimetry, Langmuir 21 (2005) 12362–12371.
[12] N. Hidalgo, C. López-López, G. Lozano, M.E. Calvo, H. Míguez, Characterization of mesoporous thin films by specular reflectance porosimetry, Langmuir 28 (2012) 13777–13782.
[13] P.C. Angelomé, L.M. Liz-Marzán, Monitoring solvent evaporation from thin films by localized surface plasmon resonance shifts, J. Phys. Chem. C 114 (2010) 18379–18383.
[14] P. Schön, R. Michalek, L. Walder, Liquid density response of a quartz crystal microbalance modified with mesoporous titanium dioxide, Anal. Chem. 71 (1999) 3305–3310.
[15] E.H. Nicollian, J.R. Brews, MOS (Metal Oxide Semiconductor) Physics and Technology 1987 Wiley, New York, 1982.
[16] R. Gregorian, G.C. Temes, Analog MOS Integrated Circuits for Signal Processing, Wiley-Interscience, New York, 1986.
[17] B.G. Streetman, S. Banerjee, Solid State Electronic Devices 4 Prentice Hall, New Jersey, 2000.
[18] M.G. Bellino, A.E. Regazzoni, G.J.A.A. Soler-Illia, Amylase-functionalized mesoporous silica thin films as robust biocatalyst platforms, ACS Appl. Mater. Interfaces 2 (2010) 360–365.
[19] G.J.A.A. Soler-Illia, P. Angelomé, M. Fuertes, A. Calvo, A. Wolosiuk, A. Zelcer, M.G. Bellino, E. Martínez, Mesoporous hybrid and nanocomposite thin films. A sol–gel toolbox to create nanoconfined systems with localized chemical properties, J. Sol-Gel Sci. Technol. 57 (2011) 299–312.
[20] N. Frančič, M.G. Bellino, G.A.A. Soler-Illia, A. Lobnik, Mesoporous titania thin films as efficient enzyme carriers for paraoxon determination/detoxification: effects of enzyme binding and pore hierarchy on the biocatalyst activity and reusability, Analyst 139 (2014) 3127–3136.
[21] D.J. Bergman, The dielectric constant of a composite material—a problem in classical physics, Phys. Rep. 43 (1978) 377–407.
[22] D.R. Ceratti, M. Faustini, C. Sinturel, M. Vayer, V. Dahirel, M. Jardat, D. Grosso, Critical effect of pore characteristics on capillary infiltration in mesoporous films, Nanoscale 7 (2015) 5371–5382.
[23] M. Mercuri, K. Pierpaulli, M.G. Bellino, C.L.A. Berli, Complex filling dynamics in mesoporous thin films, Langmuir 33 (2017) 152–157.
[24] M. Mohsen-Nia, H. Amiri, B. Jazi, Dielectric constants of water, methanol, ethanol, butanol and acetone: measurement and computational study, J. Solut. Chem. 39 (2010) 701–708.
[25] C. Hall, W.D. Hoff, Rising damp: capillary rise dynamics in walls, Proc. R. Soc. Lond. Ser. A 463 (2007) 1871–1884.
[26] N. Fries, K. Odic, M. Conrath, M. Dreyer, The effect of evaporation on the wicking of liquids into a metallic weave, J. Colloid Interface Sci. 321 (2008) 118–129.
[27] A. Rogacs, J.E. Steinbrenner, J.A. Rowlette, J.M. Weisse, X.L. Zheng, K.E. Goodson, Characterization of the wettability of thin nanostructured films in the presence of evaporation, J. Colloid Interface Sci. 349 (2010) 354–360.
[28] T. Busani, R. Devine, Dielectric and infrared properties of TiO2 films containing anatase and rutile, Semicond. Sci. Technol. 20 (2005) 870–875.
[29] H.E. Hoffman, Evaporation rates of organic liquids, Ind. Eng. Chem. 24 (1932) 135–140.
[30] V.M. Gun'ko, O.V. Goncharuk, J. Goworek, Evaporation of polar and nonpolar liquids from silica gels and fumed silica, Colloids Surf. A 474 (2015) 52–62.